

Article

Cytotoxicity Profiles and Neuroprotective Properties of the Novel Ifenprodil Analogues as Sigma Ligands

Daniele Zampieri ^{1,*}, Antonella Calabretti ¹, Maurizio Romano ², Sara Fortuna ³, Simona Collina ⁴, Emanuele Amata ⁵, Maria Dichiarà ⁵, Agostino Marrazzo ⁵ and Maria Grazia Mamolo ¹

¹ Department of Chemical and Pharmaceutical Sciences, University of Trieste, Via Giorgieri 1, 34127 Trieste, Italy; antonella.calabretti@deams.units.it (A.C.)

² Department of Life Sciences, University of Trieste, Via Valerio 28, 34127 Trieste, Italy; mromano@units.it

³ Italian Institute of Technology (IIT), Via E. Melen 83, 16152 Genova, Italy; sara.fortuna@iit.it

⁴ Department of Drug Sciences, Medicinal Chemistry and Pharmaceutical Technology Section, University of Pavia, Viale Taramelli 6 and 12, 27100 Pavia, Italy; simona.collina@unipv.it

⁵ Department of Drug and Health Sciences, University of Catania, Viale Doria 6, 95125 Catania, Italy; eamata@unict.it (E.A.)

* Correspondence: dzampieri@units.it; Tel.: +39-040-5583677

Abstract: Neurodegeneration is a slow and progressive loss of neuronal cells or their function in specific regions of the brain or in the peripheral system. Among several causes responsible for the most common neurodegenerative diseases (NDDs), cholinergic/dopaminergic pathways, but also some endogenous receptors, are often involved. In this context, sigma 1 receptor (S1R) modulators can be used as neuroprotective and anti-amnesic agents. Herein, we describe the identification of novel S1R ligands endowed with antioxidant properties, potentially useful as neuroprotective agents. We also computationally assessed how the most promising compounds might interact with the S1R protein's binding sites. The *in silico* predicted ADME properties suggested that they could be able to cross the brain-blood-barrier (BBB), and to reach the targets. Finally, the observation that at least two novel ifenprodil analogues (5d and 5i) induce an increase of the mRNA levels of the antioxidant NRF2 and SOD1 genes in SH-SY5Y cells suggests that they might be effective agents for protecting neurons against oxidative damage.

Keywords: neuroprotective agents; sigma 1 receptor; acetylcholinesterase; antioxidant properties; docking



check for updates

Citation: Zampieri, D.; Calabretti, A.; Romano, M.; Fortuna, S.; Collina, S.; Amata, E.; Dichiarà, M.; Marrazzo, A.; Mamolo, M.G. Cytotoxicity Profiles and Neuroprotective Properties of the Novel Ifenprodil Analogues as Sigma Ligands. *Molecules* **2023**, *28*, 3431. <https://doi.org/10.3390/molecules28083431>

Academic Editor: Su-Jane Wang

Received: 18 March 2023

Revised: 11 April 2023

Accepted: 11 April 2023

Published: 13 April 2023



Copyright: © 2023 by the authors. Licensee MDPI, Basel, Switzerland. This article is an open access article distributed under the terms and conditions of the Creative Commons Attribution (CC BY) license (<https://creativecommons.org/licenses/by/4.0/>).

1. Introduction

Neurodegeneration (ND) is a common final pathway present in aging and neurodegenerative diseases (NDDs), which leads to irreversible neuronal damage and death [1]. NDDs are a heterogeneous group of disorders characterized by the progressive deterioration of the structure and function of cells and their networks in the central (CNS) and peripheral nervous system [2]. Alzheimer's disease (AD), Parkinson's disease (PD), Huntington disease (HD), amyotrophic lateral sclerosis (ALS), and multiple sclerosis (MS) are the most common NDDs and the second leading cause of death worldwide in 2016 [3]. The etiopathogenesis of NDD is quite heterogeneous, and structural alterations as well as pathologically altered proteins are associated with selective dysfunctions of neurotransmitter pathways (in particular acetylcholine and dopamine systems) and progressive loss of synapses and neurons [4–6].

Besides environmental and genetic factors, oxidative stress, that leads to overproduction of reactive oxygen species (ROS), can cause neuronal death as a result of alterations of different cellular targets, such as proteostasis, mitochondria, neurotransmitter metabolism or deregulation of antioxidant pathways [7–9].

Currently, treatments for NDDs are mostly symptomatic, and there is a compelling need for novel therapies that might be potentially able to change the course of the diseases.

The N-Methyl-D-Aspartate (NMDA) receptor containing GluN2b subunit (GluN2bR) [10,11] is essential as a control unit for the glutamatergic network in the central nervous system (CNS), keeping the excitatory neurotransmission balanced [12]. Overstimulation of NMDARs, as a consequence of (S)-glutamate surfeit and the subsequent uncontrolled neuronal influx of Ca^{2+} ions, induces excitotoxicity and triggers cell death by apoptosis.

This event is one of the main causes of the onset and worsening of several NDDs including AD, PD, HA, and others. Ifenprodil (1, Figure 1) [13] is the prototypical allosteric negative modulator that interacts selectively with the GluN2bR subunit blocking the agonistic excitatory effect of glutamate. In this contest, GluN2bR inhibitors are useful to antagonize the excitotoxicity in NDDs.

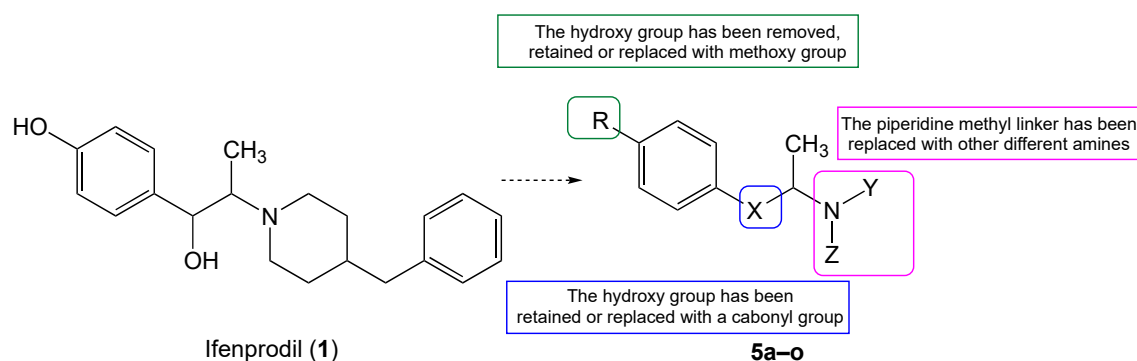


Figure 1. Rationale of the new ifenprodil analogues 5a-o.

Sigma 1 receptors (S1R) also play a relevant role in neuroprotection. They show anti-amnesic activities [14], and are involved in the modulation of opioid analgesia [15], schizophrenia without producing extrapyramidal side effects [16,17], and drug (cocaine) dependence [18]. Donepezil (Figure 2), one of the key drugs used in therapy for treating AD shows a high affinity for S1R ($K_i = 14.6$ nM) [19], although its main mechanism of action relies on inhibition of acetylcholinesterase (AChE), increasing the concentration of acetylcholine (ACh) at the synaptic level and thus restoring the cognitive functions in AD patients [20].

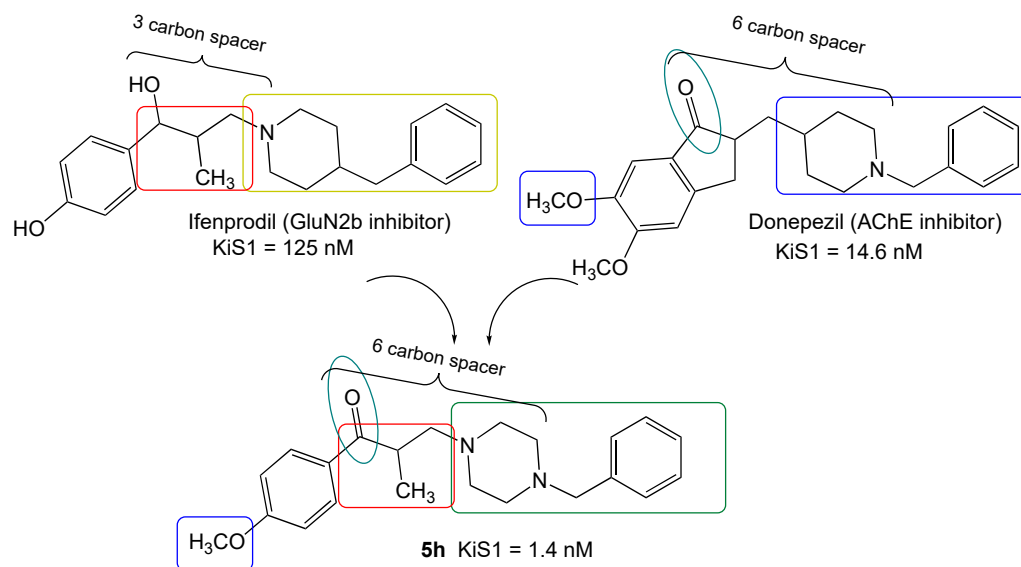


Figure 2. Molecular hybridization approach for newly synthesized compounds.

Based on these considerations, and in continuation of our efforts in discovering new SR modulators, we designed and synthesized new molecules structurally related to ifenprodil, the NMDAR modulator mentioned before, for which a moderate S1R affinity with $KiS1 = 125$ nM was also demonstrated [21].

Specifically, we designed molecules (5a–o) (Figure 1), by retaining the original phenylpropyl motif of ifenprodil, and by jointly replacing the 4-benzylpiperidine fragment with other cyclic or linear amines present in some well-known SR ligands, [22]. After in silico evaluating their drug-likeness and ability to bypass the blood-brain-barrier (BBB), all compounds have been successfully synthesized, properly characterized, and evaluated for affinity to both S1R and S2R through radioligand binding assay. Lastly, the in vitro antioxidant ability of the most interesting derivatives was evaluated as well as their potential interaction with the antioxidant response by upregulating the expression of SOD1 and NRF2 genes.

2. Results and Discussion

2.1. Compound Design

The new compounds have been designed by applying a hybridization approach, merging the key structural features of ifenprodil and donepezil. As shown in Figure 2, they present a benzylpiperazine (i.e., compound 5h) or a benzyl diazepane moiety, which can mimic the benzylpiperidine fragment of the lead AChE inhibitor donepezil, and maintain the same length of the linker between the aromatic and the aminic portion (six carbons) which ensures a good compromise to drive the affinity towards S1R as well as AChE protein.

Before the synthesis, we in silico predicted the drug-likeness properties of the designed compounds and evaluated their ability to bypass the BBB, taking into account that the final aim of this work is to discover compounds active for CNS-related pathologies.

Using the SwissADME tool (www.swissadme.ch, accessed on 18 April 2022), we in silico evaluated all compounds for a prediction of the drug-likeness properties [23], with the most common pharmacokinetic parameters, on the basis of the extended version of Lipinski's rule of five (RO5) [24]. The RO5 extended criterion means that an orally active drug should not violate more than one of the following requirements: $MW \leq 500$; HBA and HBD (related to the membrane permeability) ≤ 10 and ≤ 5 , respectively; $\log P$ and $\log S$ (related to the intestinal absorption) ≤ 5 ; $PSA \leq 140$ Å. (Table 1).

Table 1. In silico predicted main pharmacokinetic parameters of the title compounds 5a–o. Data for reference compound haloperidol (S1R ligand), ifenprodil (GluN2b ligand), and donepezil (AChE inhibitor) are reported for comparison.

Cmpd	RO5 ^a	MW ^b	HBA ^c	HBD ^d	clogP ^e	clogS ^f (mol/L)	TPSA ^g (Å < 140)	RO5 Violation	BBB Permeant	GI abs.
		<500	≤10	≤5	≤5	≤5	-	≤1	-	-
5a		322.4	3	0	3.19	−4.24	23.55	0	Yes	High
5b		294.4	4	2	2.88	−4.12	23.55	0	Yes	High
5c		295.4	2	0	4.22	−4.54	20.31	0	Yes	High
5d		308.4	3	0	2.93	−3.94	23.55	0	Yes	High
5e		352.5	4	0	3.22	−4.31	32.78	0	Yes	High
5f		324.4	3	0	2.93	−4.18	32.78	0	Yes	High
5g		325.4	3	0	4.20	−4.61	29.54	0	Yes	High
5h		338.4	4	0	2.97	−4.01	32.78	0	Yes	High
5i		338.4	4	1	2.79	−4.09	43.78	0	Yes	High
5j		311.4	3	1	3.72	−4.39	40.54	0	Yes	High
5k		324.4	4	1	2.56	−3.80	43.78	0	Yes	High
5l		310.4	3	1	2.52	−3.97	43.78	0	Yes	High
5m		297.4	2	1	3.94	−4.21	23.47	0	Yes	High
5n		327.5	3	1	3.96	−4.28	32.70	0	Yes	High

Table 1. Cont.

Cmpd	RO5 ^a	MW ^b	HBA ^c	HBD ^d	clogP ^e	clogS ^f (mol/L)	TPSA ^g (Å ² < 140)	RO5 Violation	BBB Permeant	GI abs.
		<500	≤10	≤5	≤5	≤5	-	≤1	-	-
5o		340.5	3	1	2.93	−4.16	35.94	0	Yes	High
Halo		375.9	4	1	4.22	−4.82	40.54	0	Yes	High
Ifenpr		325.4	3	2	3.41	−4.35	43.70	0	Yes	High
Donep		379.5	4	0	4.00	−4.81	38.77	0	Yes	High

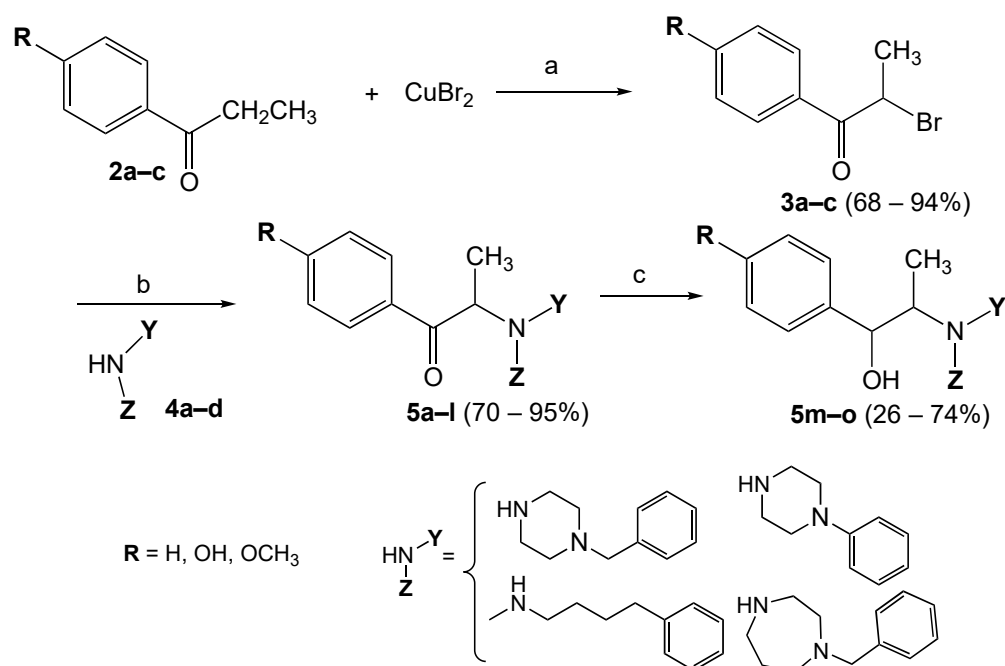
^a Lipinski's rule of five; ^b Molecular weight; ^c # of hydrogen bond acceptors; ^d # of hydrogen bond donors; ^e calculated log partition coefficient; ^f calculated log of water solubility; ^g topological polar surface area.

All the evaluated compounds **1h** and **1k–n**, in comparison with haloperidol, ifenprodil, and donepezil as references standard, exhibited good drug-likeness properties being all the values within the ranges of RO5, suggesting that our new derivatives can penetrate the BBB and reach the targets.

2.2. Chemistry

The hybrid compounds were synthesized by alkylation of substituted amines, usually present in some SR ligands, with substituted 2-bromopropiophenones.

The synthetic route is depicted in Scheme 1. It starts with the bromination of substituted propiophenones **2a–c** with CuBr₂ to afford the corresponding 2-bromopropiophenones **3a–c** in good yield (68–94%), following a slight modification of a known procedure [25]. The latter was made to react with various amines **4a–d**, in basic media, to give the final products **5a–l**. All the amines were commercially available, with the exception of 1-benzylpiperazine, which was obtained from the reaction of benzyl chloride and excess of piperazine, in THF. Reduction of the carbonyl group of compounds **5c**, **5g**, and **5e** with NaBH₄, affords the corresponding derivatives **5m–o**. All the compounds synthesized were properly characterized and all the spectra (Supplementary Materials) were in agreement with the structure predicted.



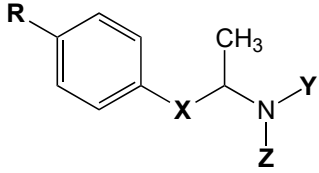
Scheme 1. Synthesis of the new compounds **5a–o**. Reagent and conditions: (a) EtOAc, 5 h, reflux; (b) ACN, K₂CO₃, KI (cat), room temperature overnight; (c) NaBH₄, EtOH, 0 °C to room temperature, 8 h.

2.3. Biology and Computational

2.3.1. SR Binding Affinities, SAR Discussion, Molecular Dynamics and Docking Studies

The S1R and S2R receptor affinities of the test compounds were determined in competition experiments by radiometric assays. The collected affinity results for the new derivatives **5a–o** are reported in Table 2.

Table 2. Binding affinities towards S1R and S2R, for compounds **5a–o**.



5a–o

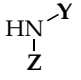
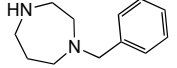
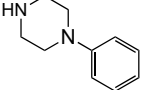
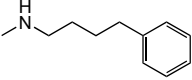
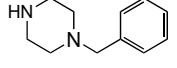
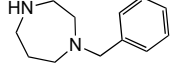
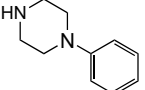
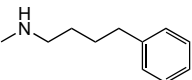
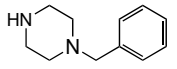
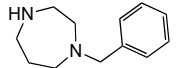
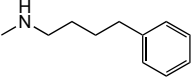
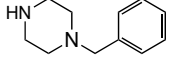
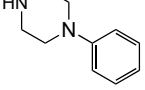
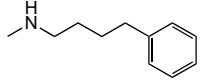
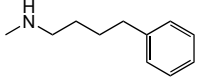
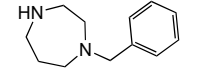
Cmpd	R	X		Ki S1R (nM) ^a	Ki S2R (nM) ^a	S2R/S1R
5a	H			69 ± 14	108 ± 21	1.6
5b	H			2931 ± 1148	158 ± 30	0.05
5c	H			4721 ± 1687	733 ± 106	0.15
5d	H			8.0 ± 1	302 ± 65	38
5e	OCH ₃	C=O		12 ± 2	97 ± 17	8.1
5f	OCH ₃			1858 ± 987	989 ± 337	0.53
5g	OCH ₃			117 ± 18	386 ± 110	3.3
5h	OCH ₃			1.4 ± 0.2	84 ± 31	60
5i	OH			19 ± 3	22 ± 4	1.1
5j	OH			121 ± 22	45 ± 4	0.38
5k	OH			19 ± 2	129 ± 23	6.8
5l	OH			785 ± 226	147 ± 17	0.18

Table 2. Cont.

5m	H			37 ± 10	30 ± 8	0.81
5n	OCH ₃	CHOH		38 ± 9	479 ± 93	13
5o	OCH ₃			4.2 ± 0.6	128 ± 26	32
Halo	-	-	-	2.6 ± 0.4	77 ± 18	30
(+)-PTZ	-	-	-	4.3 ± 0.5	1465 ± 224	312
DTG	-	-	-	124 ± 19	18 ± 1	0.14
Ifenprodil	-	-	-	125 ± 24 ^b	98 ± 34 ^b	0.75
Donepezil	-	-	-	14.6 ^c	-	-

^a Each value is the mean ± SEM of at least two experiments performed in triplicate (SRs).^b Data taken from ref. [22]. ^c Data taken from ref. [19].

Among the three subseries, the best results were achieved by benzylpiperazine-based **5d**, **5h**, and **5k** and diazepane-based **5e**, **5i**, and **5o** derivatives. Compounds **5d** and **5h**, belonging to the piperazine-based series, showed also the best selective profile with S2/S1 ratios of 38 and 60, respectively. The 4-phenylpiperazine and N-methyl-4-phenylbutylamino fragments, led to moderate results towards both SR subtypes, probably due to the shorter or longer distance between the nitrogen basic atom and the phenyl residue, respectively. Conversely, the substitution with a methoxy or hydroxy group on the aromatic portion of the phenylpropanone fragment, generally increases the affinity for both SR subtypes, with the exception of the unsubstituted compound **5d** which retains a high affinity for S1R and a favorable selectivity ratio (KiS1 = 8.0 nM and S1/S2 = 38). Among the subseries **5m–o**, the best result was achieved by diazepane-based compound **5o**, which showed high S1R affinity (KiS1 = 4.2 nM), with a 35-fold higher selectivity towards S1R with respect to the S2R subtype. Generally, the free butylamino chain led to a worse result than the related cyclic amines (diazepane and piperazine nucleus).

Experimental results were confirmed by docking a subset of compounds to the S1R protein. For all molecules, the predicted binding affinities were compatible with those measured experimentally, thus suggesting that all molecules could be potential ligands for S1R, as can be appreciated for each compound by looking at the results associated with the two largest docking clusters (Table 3).

Table 3. Comparison between experimental and docking predicted binding affinities.

Cmpd	Exp KiS1	Docking Energy Kcal/mol	Cluster Size	Predicted Kd
5d	8.0 nM	−11.36	891	4.74 nM
5o	4.2 nM	−12.31	358	0.94 nM
5h	1.4 nM	−11.72	397	2.57 nM
5i	19 nM	−11.64	219	2.92 nM
5k	19 nM	−11.48	255	3.83 nM
5e	12 nM	−12.06	487	1.43 nM

The optimum compound **5h** was further simulated for 20 ns by means of atomistic molecular dynamics (MD) simulation in full water solvent. Along the simulated time, **5h** did not leave its binding site, while it changed conformations as confirmed by visually

comparing its initial conformation, output from the docking, to the final conformation obtained at the end of the MD trajectory (Figure 3a), as well as by tracking the root mean squared deviation (RMSD) of both protein and substrate along the simulated time (Figure 3b). Its binding free energy was re-estimated by means of MMGBSA calculations over the trajectory (Figure 3c) leading to a K_d of 2.5 nM. The energy decomposition of the free energy of binding shows that the substrate is kept in place primarily by van der Waals forces (Figure 3c). Indeed, in the pocket, the substrate is surrounded by 27 residues (Figure 3d). Of the 27 closest residues, 24 residues contribute to the binding with Ile124 and Thr 181 contributing more than 2 kcal/mol (Figure 3e). Asp126, Trp164, and Glu172 instead oppose the binding. Their unfavorable contribution to the binding energy is mainly due to their high polar solvation energy which is only partially counterbalanced by a gain in electrostatic and Van der Waals (Figure 3e). This latter energetic contribution is responsible for the high binding affinity of compound 5h. An electrostatic contribution larger than 2 kcal/mol, other than those from Asp 126 and Glu172 include, that from Tyr120. Also, in this case, the polar solvation energy strongly opposes the binding, but here is counterbalanced by strong electrostatic and dispersion forces.

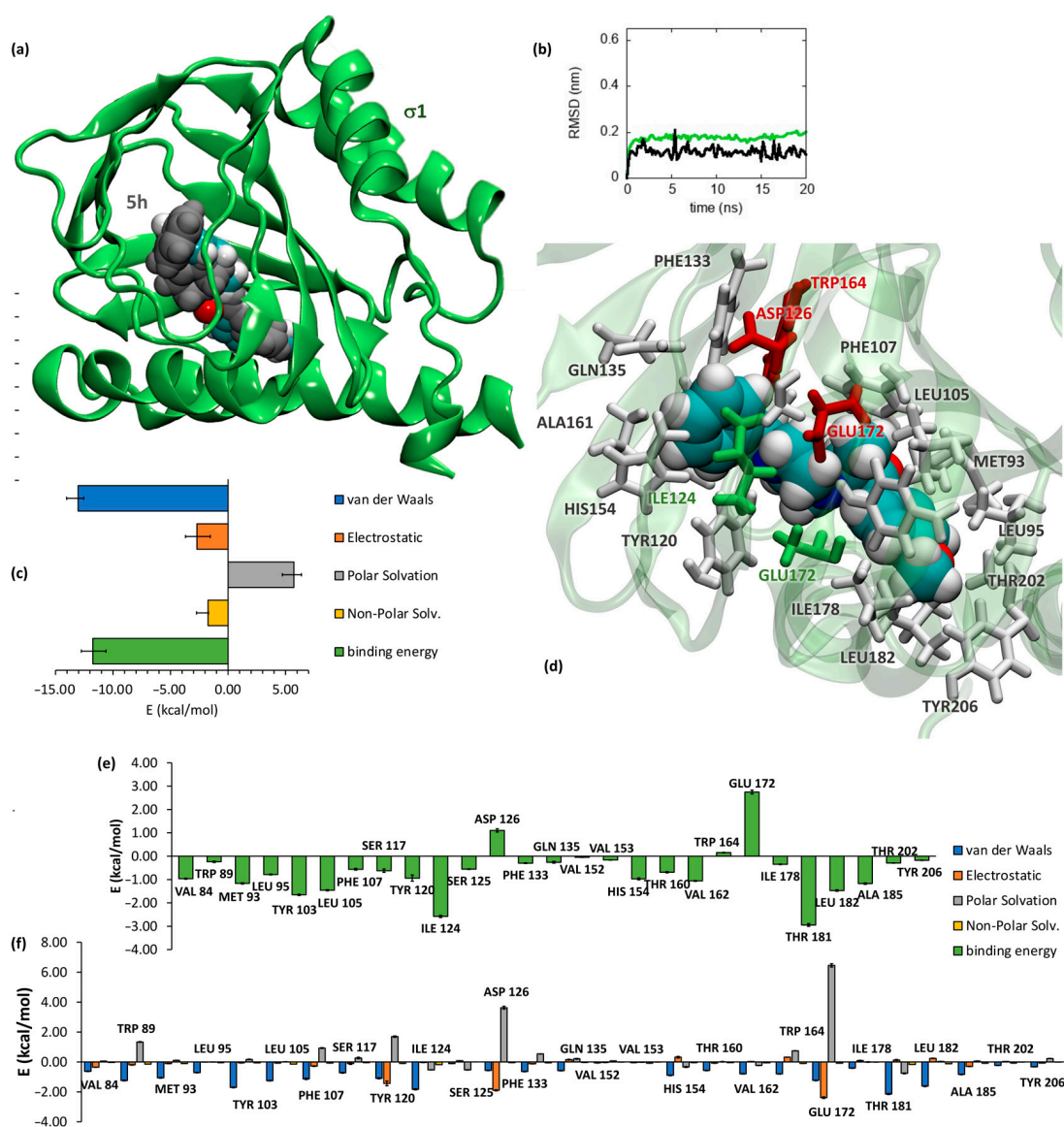


Figure 3. Computational results for compound 5h: (a) comparison between docking result and end-simulation conformation, color code: S1 (green), 5h docked conformation (cyan), 5h conformation

after 20 ns of molecular dynamics (MD) simulation (gray); (b) root mean squared deviation (RMSD) along 20 ns MD for S1 (green) and 5h (black); (c) MMGBSA calculated free energy of binding (green) and its components: Van der Waals (blue), electrostatic (orange) polar solvation (gray), and non-polar solvation (yellow), error-bars are standard deviations; (d) closest residues contribution to the binding free energy, error-bars are standard errors; (e) 5h representative conformation (at $t = 4$ ns) where S1 is shaded in green and the closest residues to 5h are highlighted and color coded as follows: contributing more than 3 kcal/mol to the binding energy (green), less than 3 kcal/mol (white), and opposing the binding (dark red); (f) energy decomposition for each residue: Van der Waals (blue), electrostatic (orange) polar solvation (gray), and non-polar solvation (yellow), error-bars are standard errors. All energy contributions in panels (c,d,f) have been calculated by MMGBSA over 20 ns MD trajectory.

2.3.2. Cytotoxic Profile

Before evaluating the antioxidant properties of compounds under investigation (5e, 5i, 5d, 5o, 5h, and 5k), we tested their cytotoxicity on the human neuroblastoma SH-SY5Y cell line, a widely used neuronal model for similar studies [26,27]. The well-known S1R antagonists NE100 and Haloperidol and the S2R agonist Siramesine have been also tested for comparative purposes.

All compounds showed toxicity < 10% at 12.5 μ M (curves are reported in Figure S1 Supplementary Materials), with IC₅₀ ranging between 74 and 294 μ M (Table 4). The lowest cytotoxic effect was shown by derivative 5i.

Table 4. IC₅₀ values for compounds 5e, 5i, 5d, 5o, 5h, and 5k.

Cmpd	IC ₅₀ (μ M)
5e	74
5i	294
5d	118
5o	118
5h	117
5k	132
Haloperidol	23
NE100	49
Siramesine	2.0

2.3.3. Effects of the Novel Ifenprodil Analogues on Antioxidant SOD1 and NRF2 in SH-SY5Y Cells

Previous studies have shown that S1 agonists (such as pentazocine) seem to attenuate oxidative stress in the retinas of rd10mice [28,29] as well as in a zebrafish model ALS of TDP-43 pathology [30] possibly by increasing the expression of the nuclear erythroid 2-related factor 2 (NRF2), a basic leucine zipper transcription factor regulating the expression of over 500 antioxidant and cytoprotective genes. In addition, it was reported that S1 agonists trigger activation of the antioxidant response elements (ARE) and cause an increase of superoxide dismutase 1 (SOD1) mRNA expression in COS cells [31].

Based on these findings, we tested the neuroprotective properties of the novel analogs by evaluating their ability to activate an antioxidant response by upregulating the expression of SOD1 and NRF2 genes. To this aim, we monitored, by Real-Time PCR, whether incubation of SH-SY5Y cells with pentazocine, haloperidol, or the compounds 5e, 5i, 5d, 5o, 5h, and 5k was associated with an increase of the mRNA levels of SOD1 and NRF2 genes. Indeed, when cells were exposed to pentazocine for 12 h, the endogenous mRNA levels of SOD1 and NRF2 raised 1.3- and 1.8-fold, respectively, as compared to DMSO treatment (Figure 4a,b). Incubation with haloperidol did not cause significant changes in mRNA levels of both genes of interest instead. The novel compounds showed a different behavior, depending on their structure: incubation with 5d was associated with a 1.3-fold increase in SOD1 mRNA levels, similar to what was observed with pentazocine.

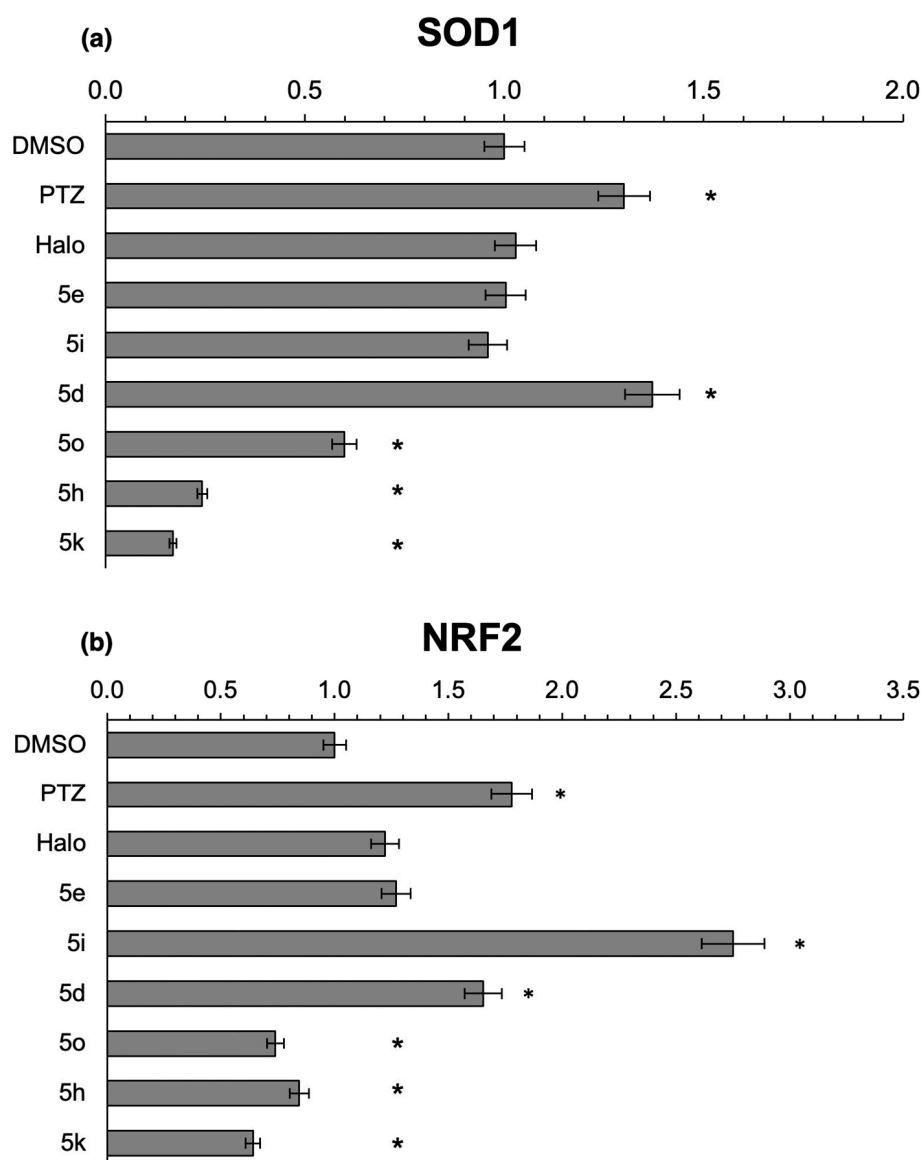


Figure 4. Effects of the novel ifenprodil analogs on (a) SOD1 and (b) NRF2 gene expression in SH-SY5Y cells. Cells were treated with pentazocine, haloperidol, or ifenprodil analogs **5e**, **5i**, **5d**, **5o**, **5h**, and **5k** (at a concentration of 12.5 μ M) for 12h, mRNA was extracted, and quantitative RT-PCR was performed to show the levels of SOD1 and of NRF2 transcripts. All data represent the mean \pm SE from triplicate independent experiments. * $p < 0.05$ vs. DMSO 1% control.

Treatment with the compounds **5e** and **5i** did not significantly alter the gene expression, whereas the compounds **5o**, **5h**, and **5k** dramatically reduced the expression of SOD1 when compared to DMSO (Figure 4a).

Concerning the effects on NRF2 expression, whereas **5e** did not change its expression significantly, **5d** and **5i** led to a 1.7-fold and 2.8-fold increase in mRNA levels of the gene (compared to DMSO). Treatment with **5o**, **5h**, and **5k** was associated with a significant decrease in gene expression (Figure 4b).

Our findings further imply that analogs **5d** and **5i** can upregulate SOD1 and NRF2 expression in human SH-SY5Y cells in a manner similar to pentazocine, suggesting that they may be useful agents for preventing oxidative damage to neurons. Conversely, **5o**, **5h**, and **5k** have been discarded since they seem to suppress both SOD1 and NRF2 expression.

2.4. Antioxidant Activity

In Vitro Intrinsic Antioxidant Activity Evaluation

Total antioxidant activities of the most interesting compounds (**5d**, **5e**, **5h**, **5i**, **5k**, and **5o**) were also evaluated by testing the ABTS (2,2'-azino-bis(3-ethylbenzothiazoline-6-sulphonic acid)) radical and hydrogen peroxide (H₂O₂) scavenging abilities. The synthetic antioxidant Trolox (6-hydroxy-2,5,7,8-tetramethylchroman-2-carboxylic acid) was used as a standard antioxidant reference. Four out of six compounds potently inhibited ABTS radicals and H₂O₂, compared to the standard (Table 5).

Table 5. Antioxidant activity of compounds **5d**, **5e**, **5h**, **5i**, **5k**, and **5o**.

Cmpd	IC ₅₀ (µg/mL) ^a	
	ABTS	H ₂ O ₂
5e	2.495 ± 0.09	12.65 ± 0.21
5i	2.603 ± 0.09	13.11 ± 0.24
5d	2.854 ± 0.11	14.56 ± 0.18
5o	2.481 ± 0.05	12.13 ± 0.25
5h	nd	466.24 ± 1.36
5k	nd	436.43 ± 1.17
Trolox	2.365 ± 0.19	15.69 ± 0.69

^a All measurements were performed in triplicate, and data were expressed as mean value ± SD; nd: not determined.

Compounds **5d**, **5e**, **5i**, and **5o**, exhibited a significant radical scavenging capacity both on the ABTS and H₂O₂, with IC₅₀ values comparable to Trolox. All the diazepane-based compounds tested showed the best scavenging property.

3. Materials and Methods

3.1. Chemistry

3.1.1. Chemical Reagents and Instruments

All reagents and solvents were of analytical grade and used as received. Flash chromatography was performed using Silica Gel 60 (70–230 mesh, Merck, Milan, Italy). Reaction courses were monitored on precoated silica gel TLC-GF₂₅₄ plates (Merck) and spots were visualized under ultraviolet light at 254 nm or iodine vapors. Melting points (°C) were determined with a Stuart SMP 300 apparatus in open glass capillaries and were uncorrected. Agilent Cary-60 spectrophotometer UV-Vis was employed to record the spectra and quantify the absorbance. Infrared spectra were recorded on an FTIR Jasco 4700 spectrophotometer in nujol mulls. Nuclear magnetic resonance spectra were obtained on a Varian 400 MHz. Chemical shifts are reported as δ (ppm) in CDCl₃ solution related to tetramethyl silane as an internal standard; 1 drop of D₂O was added to assign NH or OH protons. ¹H-¹H coupling constants (*J*) are given in Hz and the splitting abbreviations used are *s*, singlet; *d*, doublet; *dd*, doublet of doublets; *ddd*: doublet of doublet of doublets; *t*, triplet; *tt*, triplet of triplets; *dt*, doublet of triplets; *q*, quartet; *m*, multiplet. Microanalyses (C, H, N) were carried out with Elementar Vario ELIII apparatus and were in agreement with theoretical values ±0.4%. ESI-MS spectra were recorded on a Bruker Daltonics Esquire 4000 spectrometer (MeOH ultrapure as solvent).

3.1.2. Synthetic Procedure

General Synthesis of Brominated Compounds **3a–c**

2-Bromo-1-phenylpropan-1-one (**3a**)

CuBr₂ (10.0 g 44.7 mmol, 2eq) was dissolved in 100 mL of EtOAc and heated at reflux temperature on a magnetic stirrer hot plate, then 3.0 g of propiophenone **2a** (22.4 mmol, 1 eq) was added. At reaction completion (the color of the solution changed from green to amber; TLC: CH₂Cl₂/EtOH 95:5) the inorganic salt of copper (I) bromide was collected

by filtration and washed with fresh EtOAc. The organic phase was washed with water (3 × 100 mL) at neutrality, dried over MgSO₄, filtered, and evaporated to dryness to give a chromatographically pure yellow oil **3a**.

Yield: 4.35 g, 91%. Rf: 0.79 (CH₂Cl₂/EtOH 95:5). ¹H-NMR (400 MHz, CDCl₃): δ 8.06–7.98 (m, 2H, arom.), 7.63–7.52 (m, 1H, arom.), 7.53–7.41 (m, 2H, arom.), 5.29 (q, J = 6.6 Hz, 1H, CH), 1.90 (d, J = 6.6 Hz, 3H, CH₃). MS-ESI: [M+H]⁺ = 213, [M+H+2]⁺ = 215.

With the same procedure, but starting from 4-hydroxypropiofenone and 4-methoxy propiofenone, compounds **3b** and **3c** were obtained.

2-Bromo-1-(4-methoxyphenyl)propan-1-one (**3b**)

Whitish solid, yield: 2.02 g, 68%. Mp: 62–64 °C. Rf: 0.64 (CH₂Cl₂). ¹H-NMR (400 MHz, CDCl₃): δ 8.05–7.96 (m, 2H, arom.), 6.99–6.90 (m, 2H, arom.), 5.26 (q, J = 6.6 Hz, 1H, CH), 3.87 (s, 3H, OCH₃), 1.88 (d, J = 6.6 Hz, 3H, CH₃). MS-ESI: [M+H]⁺ = 243, [M+H+2]⁺ = 245.

2-Bromo-1-(4-hydroxyphenyl)propan-1-one (**3c**)

Light brown solid, yield: 2.86 g, 94%. Mp: 90–92 °C. Rf: 0.63 (CH₂Cl₂). ¹H-NMR (400 MHz, CDCl₃): δ 7.97 (d, J = 8.8 Hz, 2H, arom.), 6.92 (d, J = 8.9 Hz, 2H, arom.), 6.14 (s, 1H, OH), 5.25 (q, J = 6.6 Hz, 1H, CH), 1.89 (d, J = 6.6 Hz, 3H, CH₃). MS-ESI: [M+H]⁺ = 229, [M+H+2]⁺ = 231.

General Synthesis of the Final Compounds **5a–m**

2-(4-Benzyl-1,4-diazepan-1-yl)-1-phenylpropan-1-one (**5a**)

On an ice bath (0 °C), a 100 mL round bottom flask with a mixture of 203 mg of compound **3a** (0.95 mmol, 1 eq), 181 mg (0.95 mmol, 1 eq) of *N*-benzylomopiperazine (1-benzyl-1,4-diazepane) **4a**, 198 mg (1.42 mmol, 1.5 eq) of K₂CO₃, a catalytic amount of KI and 50 mL of ACN, was left to stir overnight. At reaction completion, the inorganic salts were collected by filtration, and the organic phase was washed with distilled water (3 × 30 mL), dried over MgSO₄, filtered, and evaporated under reduced pressure. No further purification was required.

Yellow oil, yield: 264 mg, 81%. FT-IR (cm⁻¹): 1679. ¹H-NMR (400 MHz, CDCl₃): δ 8.10–8.03 (m, 2H, arom.), 7.60–7.37 (m, 3H, arom.), 7.38–7.16 (m, 3H, arom.), 4.27 (q, J = 6.7 Hz, 1H, CH), 3.55 (s, 2H, CH₂), 2.89–2.71 (m, 4H, CH₂, diazep.), 2.63–2.55 (m, 3H, CH₂, diazep.), 2.46 (ddd, J = 12.8, 7.2, 3.2 Hz, 1H, CH₂ diazep.), 1.80–1.60 (m, 2H, CH₂ diazep.), 1.25 (d, J = 6.7 Hz, 3H, CH₃). ¹³C-NMR (101 MHz, CDCl₃): δ 200.89, 139.47, 136.59, 132.63, 128.88, 128.76, 128.17, 128.10, 126.75, 64.10, 62.02, 56.38, 53.89, 50.85, 50.57, 28.46, 10.18. MS-ESI: [M+H]⁺ = 323; elemental analysis calcd (%) for C₂₁H₂₆N₂O: C 78.22, H 8.13, N 8.69; found: C 78.10, H 8.35, N 8.50.

In addition to *N*-benzylomopiperazine, 1-phenylpiperazine, *N*-methyl-4-phenylbutan-1-amine, and 1-benzylpiperazine were used to afford compounds **5b–l**.

2-(4-Phenylpiperazin-1-yl)-1-phenylpropan-1-one (**5b**)

Brown solid, yield: 228.4 mg, 81%. Mp: 105–106 °C. Rf: 0.41 (CH₂Cl₂). FT-IR (cm⁻¹): 1679. ¹H-NMR (400 MHz, CDCl₃): δ 8.17–8.09 (m, 2H, arom.), 7.61–7.51 (m, 1H, arom.), 7.50–7.41 (m, 2H, arom.), 7.30–7.21 (m, 2H, arom.), 6.96–6.80 (m, 3H, arom.), 4.16 (q, J = 6.8 Hz, 1H, CH), 3.25–3.10 (m, 4H, CH₂ pip.), 2.86–2.68 (m, 4H, CH₂ pip.), 1.34 (d, J = 6.8 Hz, 3H, CH₃). ¹³C-NMR (101 MHz, CDCl₃): δ 200.34, 151.31, 136.26, 133.01, 129.06, 128.88, 128.40, 119.72, 116.10, 64.55, 49.63, 49.47, 11.64. MS-ESI: [M+H]⁺ = 295, [M+Na]⁺ = 317; elemental analysis calcd (%) for C₁₉H₂₂N₂O: C 77.52, H 7.53, N 9.52; found: C 77.75, H 7.50, N 9.55.

2-(Methyl(4-phenylbutyl)amino)-1-phenylpropan-1-one (**5c**)

Yellow oil, yield: 230 mg, 80 %. Rf: 0.25 (CH₂Cl₂/EtOH 95:5). FT-IR (cm⁻¹): 1677. ¹H-NMR (400 MHz, CDCl₃): δ 8.11–8.03 (m, 2H, arom.), 7.60–7.46 (m, 1H, arom.), 7.47–7.38 (m, 2H, arom.), 7.33–7.22 (m, 2H, arom.), 7.27–7.13 (m, 1H, arom.), 7.18–7.06 (m, 2H, arom.), 4.22 (q, J = 6.7 Hz, 1H, CH), 2.68–2.42 (m, 4H, NCH₂CH₂CH₂CH₂), 2.26 (s, 3H, NCH₃),

1.64–1.42 (m, 4H, NCH₂CH₂CH₂CH₂), 1.25 (d, *J* = 6.7 Hz, 3H, CH₃). ¹³C-NMR (101 MHz, CDCl₃): δ 200.91, 142.49, 136.58, 132.69, 128.90, 128.40, 128.35, 128.34, 128.27, 128.20, 125.94, 125.61, 63.42, 53.68, 37.69, 35.66, 28.85, 28.59, 27.38, 9.40. MS-ESI: [M+H]⁺ = 296; elemental analysis calcd (%) for C₂₀H₂₅NO: C 81.31, H 8.53, N 4.74; found: C 81.45, H 8.33, N 4.62.

2-(4-Benzylpiperazin-1-yl)-1-phenylpropan-1-one (5d)

Yellow oil, yield: 182 mg, 80%. Rf: 0.21 (CH₂Cl₂/EtOH 95:5). FT-IR (cm⁻¹): 1685. ¹H-NMR (400 MHz, CDCl₃): δ 8.13–8.05 (m, 2H, arom.), 7.62–7.39 (m, 3H, arom.), 7.35–7.19 (m, 5H, arom.), 4.09 (q, *J* = 6.8 Hz, 1H, CH), 3.50 (s, 2H, CH₂), 2.78–2.56 (m, 4H, CH₂ pip.), 2.48 (s, 4H, CH₂ pip.), 1.28 (d, *J* = 6.8 Hz, 3H, CH₃). ¹³C-NMR (101 MHz, CDCl₃): δ 200.43, 136.28, 132.91, 129.28, 128.85, 128.83, 128.70, 128.66, 128.34, 128.22, 127.15, 109.99, 64.44, 62.91, 53.23, 49.41, 11.68. MS-ESI: [M+H]⁺ = 309; elemental analysis calcd (%) for C₂₀H₂₄N₂O: C 77.89, H 7.84, N 9.08; found: C 77.70, H 7.90, N 9.05.

2-(4-Benzyl-1,4-diazepan-1-yl)-1-(4-methoxyphenyl)propan-1-one (5e)

Light brown oil, yield: 248 mg, 83%. Rf: 0.40 (CH₂Cl₂/EtOH 95:5). FT-IR (cm⁻¹): 1675. ¹H-NMR (400 MHz, CDCl₃): δ 8.13–8.04 (m, 2H, arom.), 7.35–7.16 (m, 5H, arom.), 6.95–6.87 (m, 2H, arom.), 4.22 (q, *J* = 6.7 Hz, 1H, CH), 3.86 (d, *J* = 0.6 Hz, 3H, OCH₃), 3.57 (s, 2H, CH₂), 2.89–2.68 (m, 4H, CH₂, diazep.), 2.70–2.56 (m, 3H, CH₂, diazep.), 2.48 (ddd, *J* = 12.7, 6.8, 3.6 Hz, 1H, CH₂, diazep.), 1.81–1.61 (m, 2H, CH₂, diazep.), 1.24 (d, *J* = 6.7 Hz, 3H, CH₃). ¹³C-NMR (101 MHz, CDCl₃): δ 199.41, 163.12, 139.49, 131.25, 129.44, 128.77, 128.09, 126.75, 113.62, 113.31, 63.98, 62.09, 56.43, 55.38, 53.90, 50.85, 50.61, 28.46, 10.39. MS-ESI: [M+H]⁺ = 353, [M+Na]⁺ = 375; elemental analysis calcd (%) for C₂₂H₂₈N₂O₂: C 74.97, H 8.01, N 7.95; found: C 74.70, H 8.15, N 8.05.

2-(4-Phenylpiperazin-1-yl)-1-(4-methoxyphenyl)propan-1-one (5f)

Light brown solid, yield: 230 mg, 86%; Mp: 117–119 °C. Rf: 0.42 (CH₂Cl₂/EtOH 95:5). FT-IR (cm⁻¹): 1680. ¹H-NMR (400 MHz, CDCl₃): δ 8.19–8.08 (m, 2H, arom.), 7.31–7.19 (m, 2H, arom.), 6.98–6.79 (m, 5H, arom.), 4.08 (q, *J* = 6.8 Hz, 1H, CH), 3.87 (s, 3H, OCH₃), 3.29–3.09 (m, 4H, CH₂ pip.), 2.85–2.66 (m, 4H, CH₂ pip.), 1.33 (d, *J* = 6.8 Hz, 3H, CH₃). ¹³C-NMR (101 MHz, CDCl₃): δ 198.94, 163.42, 151.32, 131.26, 129.13, 129.05, 119.68, 116.07, 113.53, 64.62, 55.44, 49.72, 49.45, 12.08. MS-ESI: [M+H]⁺ = 325; elemental analysis calcd (%) for C₂₀H₂₄N₂O₂: C 74.05, H 7.46, N 8.63; found: C 74.00, H 7.52, N 8.57.

1-(4-Methoxyphenyl)-2-(methyl(4-phenylbutyl)amino)propan-1-one (5g)

Yellow oil, yield: 259 mg, 94%. Rf: 0.29 (CH₂Cl₂/EtOH 95:5). FT-IR (cm⁻¹): 1675. ¹H-NMR (400 MHz, CDCl₃): δ 8.13–8.05 (m, 2H, arom.), 7.30–7.06 (m, 5H, arom.), 6.99–6.83 (m, 2H, arom.), 4.17 (q, *J* = 6.7 Hz, 1H, CH), 3.82 (s, 3H, OCH₃), 2.69–2.43 (m, 4H, NCH₂CH₂CH₂CH₂), 2.26 (s, 3H, NCH₃), 1.62–1.44 (m, 4H, NCH₂CH₂CH₂CH₂), 1.24 (d, *J* = 6.7 Hz, 3H, CH₃). ¹³C-NMR (101 MHz, CDCl₃): δ 199.34, 163.23, 142.51, 133.93, 131.29, 131.03, 129.37, 128.34, 128.26, 128.20, 125.61, 113.43, 113.22, 63.44, 55.48, 55.35, 53.63, 37.85, 37.69, 35.64, 28.84, 27.33, 9.63. MS-ESI: [M+H]⁺ = 326; elemental analysis calcd (%) for C₂₁H₂₇NO₂: C 77.50, H 8.36, N 4.30; found: C 77.55, H 8.30, N 4.25.

2-(4-Benzylpiperazin-1-yl)-1-(4-methoxyphenyl)propan-1-one (5h)

Brownish solid, yield: 138 mg, 69%. Mp: 80–82 °C. Rf: 0.42 (CH₂Cl₂/EtOH 95:5). FT-IR (cm⁻¹): 1675. ¹H-NMR (400 MHz, CDCl₃): δ 8.15–8.07 (m, 2H, arom.), 7.30 (d, *J* = 4.4 Hz, 4H, arom.), 7.27–7.20 (m, 1H, arom.), 6.99–6.88 (m, 2H, arom.), 4.01 (q, *J* = 6.7 Hz, 1H, CH), 3.87 (s, 3H, OCH₃), 3.49 (s, 2H, CH₂), 2.70–2.61 (m, 2H, CH₂ pip.), 2.59 (m, 2H, CH₂ pip.), 2.49 (d, *J* = 12.4 Hz, 4H, CH₂ pip.), 1.27 (d, *J* = 6.8 Hz, 3H, CH₃). ¹³C-NMR (101 MHz, CDCl₃): δ 199.06, 163.33, 131.28, 131.21, 129.23, 129.21, 128.19, 127.07, 113.94, 113.46, 109.99, 64.53, 62.95, 55.41, 53.27, 12.09. MS-ESI: [M+H]⁺ = 339; elemental analysis calcd (%) for C₂₁H₂₆N₂O₂: C 74.53, H 7.74, N 8.28; found: C 74.65, H 7.55, N 8.18

2-(4-Benzyl-1,4-diazepan-1-yl)-1-(4-hydroxyphenyl)propan-1-one (5i)

Light brown oil, yield: 228 mg, 74 %. Rf: 0.15 (CH₂Cl₂). FT-IR (cm⁻¹): 3332, 1652. ¹H-NMR (400 MHz, CDCl₃): δ 7.92 (d, *J* = 8.6 Hz, 2H, arom.), 7.28–7.21 (m, 5H, arom.), 7.15 (s all, 1H, OH), 6.77 (d, *J* = 8.5 Hz, 2H, arom.), 4.24 (q, *J* = 6.7 Hz, 1H, CH), 3.63 (s, 2H, CH₂), 2.85 (ddd, *J* = 18.0, 8.0, 3.5 Hz, 4H, CH₂, diazep.), 2.71 (dt, *J* = 10.1, 5.3 Hz, 3H, CH₂, diazep.), 2.70–2.54 (m, 1H, CH₂, diazep.), 1.86–1.75 (m, 2H, CH₂, diazep.), 1.23 (d, *J* = 6.7 Hz, 3H, CH₃). ¹³C-NMR (101 MHz, CDCl₃): δ 199.58, 162.36, 137.45, 131.45, 129.39, 128.31, 127.82, 127.33, 115.66, 63.23, 61.83, 55.80, 53.62, 50.72, 49.38, 27.31, 11.40. MS-ESI: [M+H]⁺ = 339; elemental analysis calcd (%) for C₂₁H₂₆N₂O₂: C 74.53, H 7.74, N 8.28; found: C 74.30, H 7.85, N 8.35.

1-(4-Hydroxyphenyl)-2-(methyl(4-phenylbutyl)amino)propan-1-one (5j)

Light brown oil, yield: 198 mg, 70 %. Rf: 0.50 (CH₂Cl₂/EtOH 90:10). FT-IR (cm⁻¹): 3330, 1660. ¹H-NMR (400 MHz, CDCl₃): δ 7.97 (dq, *J* = 8.9, 3.5, 3.1 Hz, 2H, arom.), 7.30–7.05 (m, 5H, arom.), 6.92–6.75 (m, 2H, arom.), 5.53 (s, 1H, OH), 4.23–4.07 (m, 1H, CH), 2.62–2.43 (m, 4H, NCH₂CH₂CH₂CH₂), 2.28 (s, 3H, NCH₃), 1.78–1.43 (m, 4H, NCH₂CH₂CH₂CH₂), 1.28–1.16 (m, 3H, CH₃). ¹³C-NMR (101 MHz, CDCl₃): δ 199.69, 142.40, 131.50, 128.34, 128.32, 128.20, 125.85, 125.60, 115.42, 62.92, 53.90, 37.85, 35.62, 28.93, 27.05, 10.94. MS-ESI: [M+H]⁺ = 312; elemental analysis calcd (%) for C₂₀H₂₅NO₂: C 77.14, H 8.09, N 4.50; found: C 77.05, H 7.93, N 4.55.

2-(4-Benzylpiperazin-1-yl)-1-(4-hydroxyphenyl)propan-1-one (5k)

Whitish solid, yield: 151 mg, 71%. Mp: 58–59 °C. Rf: 0.26 (CH₂Cl₂/EtOH 95:5). FT-IR (cm⁻¹): 3325, 1672. ¹H-NMR (400 MHz, CDCl₃): δ 8.03–7.87 (m, 2H, arom.), 7.34–7.20 (m, 5H, arom.), 6.90–6.72 (m, 2H, arom.), 4.06–3.91 (m, 1H, CH), 3.56–3.48 (m, 2H, CH₂), 2.69–2.43 (m, 8H, CH₂ pip.), 1.30–1.19 (m, 3H, CH₃). ¹³C-NMR (101 MHz, CDCl₃): δ 198.99, 161.01, 131.45, 131.34, 129.57, 129.47, 128.62, 128.30, 127.40, 115.45, 63.83, 62.85, 53.00, 52.58, 12.98. MS-ESI: [M+H]⁺ = 325; elemental analysis calcd (%) for C₂₀H₂₄N₂O₂: C 74.05, H 7.46, N 8.63; found: C 74.20, H 7.35, N 8.44.

2-(4-Phenylpiperazin-1-yl)-1-(4-hydroxyphenyl)propan-1-one (5l)

Purified through *flash chromatography* (CH₂Cl₂/EtOH 98:2). Brown solid, yield: 83.0 mg, 47%. Mp: 163–165 °C. Rf: 0.75 (CH₂Cl₂/EtOH 95:5). FT-IR (cm⁻¹): 3338, 1655. ¹H-NMR (400 MHz, CDCl₃): δ 8.11–8.02 (m, 2H, arom.), 7.35–7.19 (m, 2H, arom.), 6.95–6.80 (m, 5H, arom.), 4.11 (q, *J* = 6.8 Hz, 1H, CH), 3.20 (dt, *J* = 6.7, 3.5 Hz, 4H, CH₂ pip.), 2.83 (dt, *J* = 10.6, 4.9 Hz, 2H, CH₂ pip.), 2.74 (dt, *J* = 10.9, 5.0 Hz, 2H, CH₂ pip.), 1.34 (d, *J* = 6.8 Hz, 3H, CH₃). ¹³C-NMR (101 MHz, CDCl₃): δ 198.96, 160.37, 151.15, 131.54, 129.08, 119.90, 116.19, 115.29, 64.43, 49.78, 49.37, 12.50. MS-ESI: [M+H]⁺ = 311; elemental analysis calcd (%) for C₁₉H₂₂N₂O₂: C 73.52, H 7.14, N 9.03; found: C 73.45, H 7.25, N 9.15.

General Synthesis for the Reduced Compounds **5m–o***2-(Methyl(4-phenylbutyl)amino)-1-phenylpropan-1-ol (5m)*

To a stirred solution of 2-(*methyl(4-phenylbutyl)amino*)-1-phenylpropan-1-one **5c** (100 mg, 0.34 mmol, 1 eq) in abs, EtOH (20 mL) at 0 °C and 25.2 mg of NaBH₄ (0.68 mmol, 2eq) were added portion-wise. The reaction mixture was allowed to reach room temperature and stirred for a further 8 h. The solvent was removed under reduced pressure, and water was added to the residue. The aqueous layer was extracted with CH₂Cl₂ (3 × 20 mL). The combined organic layers were dried (MgSO₄), filtered, and concentrated in a vacuum to obtain **5m** as a yellow oil, chromatographically pure.

Yield: 75 mg, 74%. Rf: 0.54 (CH₂Cl₂/EtOH 90:10). FT-IR (cm⁻¹): 3389. ¹H-NMR (400 MHz, CDCl₃): δ 7.33–7.15 (m, 10H, arom.), 4.81 (d, *J* = 4.4 Hz, 1H, CHOH), 2.80 (qd, *J* = 6.9, 4.0 Hz, 1H, CHCH₃), 2.62 (t, *J* = 7.4 Hz, 2H, NCH₂CH₂CH₂CH₂), 2.51–2.31 (m, 2H, NCH₂CH₂CH₂CH₂), 2.24 (s, 3H, NCH₃), 1.67–1.44 (m, 4H, NCH₂CH₂CH₂CH₂), 1.27 (s, 1H, OH), 0.86 (d, *J* = 6.8 Hz, 3H, CH₃). ¹³C-NMR (101 MHz, CDCl₃): δ 142.41, 142.32, 128.37,

128.28, 127.90, 126.80, 126.06, 125.70, 72.87, 63.52, 54.73, 38.84, 35.81, 29.70, 29.01, 27.01, 10.02. MS-ESI: $[M+H]^+ = 298$; elemental analysis calcd (%) for $C_{20}H_{27}NO$: C 80.76, H 9.15, N 4.71; found: C 80.85, H 9.03, N 4.66.

The same procedure was adopted to obtain derivatives **5n,o**.

1-(4-Methoxyphenyl)-2-(methyl(4-phenylbutyl)amino)propan-1-ol (5n)

Dark yellow oil, yield: 32.4 mg, 32%. Rf: 0.59 ($CH_2Cl_2/EtOH$ 90:10). FT-IR (cm^{-1}): 3389. 1H -NMR (400 MHz, $CDCl_3$): δ 7.34–7.21 (m, 4H, arom.), 7.26–7.14 (m, 4H, arom.), 6.93–6.81 (m, 2H, arom.), 4.17 (d, $J = 9.7$ Hz, 1H, $CHOH$), 3.80 (s, 3H, OCH_3), 2.70–2.34 (m, 4H, $NCH_2CH_2CH_2CH_2$), 2.23 (s, 3H, NCH_3), 1.76–1.50 (m, 4H, $NCH_2CH_2CH_2CH_2$), 1.34–1.24 (m, 1H, OH), 0.87 and 0.71 (d, $J = 6.8$ Hz, 3H, CH_3). ^{13}C -NMR (101 MHz, $CDCl_3$): δ 159.14, 142.40, 134.39, 134.21, 128.41, 128.29, 127.16, 125.71, 113.62, 113.34, 74.19, 65.58, 55.25, 38.81, 35.81, 29.03, 27.78, 26.99, 7.19. MS-ESI: $[M+H]^+ = 328$, $[M+Na]^+ = 350$; elemental analysis calcd (%) for $C_{21}H_{29}NO_2$: C 77.02, H 8.93, N 4.28; found: C 77.05, H 8.83, N 4.15.

2-(4-Benzyl-1,4-diazepan-1-yl)-1-(4-methoxyphenyl)propan-1-ol (5o)

Yellow oil, yield: 28.4 mg, 26%. Rf: 0.26 ($CH_2Cl_2/EtOH$ 95:5). FT-IR (cm^{-1}): 3389. 1H -NMR (400 MHz, $CDCl_3$): δ 7.39–7.23 (m, 5H, arom.), 7.28–7.16 (m, 2H, arom.), 6.90–6.83 (m, 2H, arom.), 4.14 (d, $J = 9.7$ Hz, 1H, $CHOH$), 3.80 (s, 3H, OCH_3), 3.67 (s, 2H, CH_2), 2.94–2.57 (m, 9H, $4 \times CH_2$ diazep. and $CHCH_3$), 1.87 (tt, $J = 12.2, 10.7, 4.4$ Hz, 2H, CH_2 diazep.), 1.25 (s, 1H, OH), 0.76 (d, $J = 6.6$ Hz, 3H, CH_3). ^{13}C -NMR (101 MHz, $CDCl_3$): δ 159.14, 133.94, 128.83, 128.40, 128.21, 126.92, 113.63, 74.38, 67.70, 62.78, 56.76, 55.24, 53.95, 28.46, 8.45. MS-ESI: $[M+H]^+ = 355$; elemental analysis calcd (%) for $C_{22}H_{30}N_2O_2$: C 74.54, H 8.53, N 7.90; found: C 74.25, H 8.50, N 7.95.

3.2. Computational

3.2.1. Docking

S1 protein was modeled by homology by using as a template chain A from PDB 5HK2 [32]. Details on the followed procedure can be found in [22]. Ligands were minimized with the AM1 method with MOPAC [33] and prepared with AutoDock tools. Docking was performed with AutoDock [34]. The docking box was centered on the ligand cocrystallized in 5HK2. A grid of $40 \times 42 \times 40$ points with spacing 0.375 \AA was employed. The docking was based on the Lamarckian Genetic Algorithm with 1000 runs and 2,500,000 maximum numbers of evaluations. The representative conformation of the largest cluster was selected for subsequent analysis.

3.2.2. Molecular Dynamics

The minimization of the complex was performed in subsequent steps by constraining the selected portion of the systems. First side chains were minimized, then the whole protein, then the whole system. The system was then placed in a cubic box with periodic boundary conditions, and a 0.7 nm water layer was added before performing a further minimization. We used AMBER99SB force field and tip3p water. Ligand topologies were built with Antechamber [35] and converted into GROMACS topologies [36]. The 100 ps long NVT and NPT equilibrations were performed by constraining the protein backbone. NPT production runs of 20 ns of the unconstrained system were run at 300 K and 1 atm. A modified Berendsen thermostat and Parinello–Rahman pressure coupling were employed. The iteration time step was set to 2 fs with the leap-frog integrator and LINCS [37] constraint. Sampled conformations were clustered with the Daura algorithm [38] cutoff of 0.05 nm. RMSDs have been calculated from configurations sampled every 10 ps. All simulations and their analyses were performed with the Gromacs package v. 2021 [39]. The binding free energy was estimated with the MM/GBSA method by using the *gmx_MMPBSA* tool [40]. Apolar solvation energies were calculated as solvent-accessible surface area (SASA). All calculations were run on M100 (CINECA, Bologna, Italy).

3.3. Hydrogen Peroxide Radical Scavenging Activity

The compounds' antioxidant capacity was evaluated by bleaching the green colored ethanolic solution of ABTS [41]. Test compounds (300 μ L) were diluted as follows: 0.01, 0.025, 0.05, 0.1, and 0.2 mg/mL and added to 2.7 mL of ethanolic solution of ABTS (7 mM). These mixtures were incubated for 45 min at room temperature, and the absorbances were recorded at $\lambda = 735$ nm against the ABTS solution. The results were obtained as the percent of inhibition (% IC) of ABTS radical, calculated by the following formula.

$$\% \text{ IC} = [(\text{Abs ABTS} - \text{Abs Sample}) / \text{Abs ABTS}] \times 100$$

Data were expressed as mean value \pm SD, and the assay was performed in triplicate. The % IC was used to determine the IC₅₀ values.

The ABTS method was applied also to measure the IC₅₀ of H₂O₂ (2 mM, $\lambda = 230$ nm), used as an oxidant compound comparing values.

3.4. Biology

3.4.1. S1R and S2R Binding Assays

Materials

Brain and liver homogenates for S1R and S2R receptor binding assays were prepared from male Dunkin-Hartley guinea pigs and Sprague Dawley rats, respectively (ENVIGO RMS S.R.L., Udine, Italy; Italian Minister of Health, authorization for animal experimentation—Project acronym 335/1984F.N.JLT). [³H](+)-pentazocine (26.9 Ci/mmol) and [³H]1,3-di-*o*-tolylguanidine ([³H]DTG, 35.5 Ci/mmol) were purchased from PerkinElmer (Zaventem, Belgium). Ultima Gold MV Scintillation cocktail was from PerkinElmer (Milan, Italy). All the other materials were obtained from Merck Life Science S.r.l. (Milan, Italy). UV absorbance was measured using a microplate spectrophotometer reader (Synergy HT, Biotec). The bound radioactivity has been determined using a Beckman LS 6500 liquid scintillation counter (Beckman Coulter, Brea, CA, USA).

Preparation of the Test Compounds

The test compound solutions were prepared by dissolving approximately 10 μ mol of the test compound in DMSO to obtain a 10 mM stock solution. The required final concentrations for the assay (from 10⁻⁵ to 10⁻¹¹ M) have been reached by diluting the DMSO stock solution with the respective assay buffer.

Preparation of the Membranes from Pig Brain

Fresh guinea pig brain cortex was homogenized in ice-cold Tris (50 mM, pH 7.4) containing cold 0.32 M sucrose with a Potter-Elvehjem glass homogenizer. The suspension was centrifuged at 1030 $\times g$ for 10 min at 4 $^{\circ}$ C. The supernatant was separated and centrifuged at 41,200 $\times g$ for 20 min at 4 $^{\circ}$ C. The obtained pellet was suspended in ice-cold Tris (50 mM, pH 7.4), incubated at room temperature for 15 min, and centrifuged again at 41,200 $\times g$ for 15 min at 4 $^{\circ}$ C. The final pellet was resuspended in ice-cold Tris buffer, and frozen at -80 $^{\circ}$ C. The protein concentration was determined by the method of Bradford [42].

Preparation of the Membranes from Rat Liver

A few rat livers were homogenized in cold 0.32 M sucrose with a Potter-Elvehjem glass homogenizer. The suspension was centrifuged at 1030 $\times g$ for 10 min at 4 $^{\circ}$ C. The supernatant was separated and centrifuged at 31,100 $\times g$ for 20 min at 4 $^{\circ}$ C. The pellet was resuspended in ice-cold Tris buffer (50 mM, pH 8) and incubated at room temperature for 30 min. Then, the suspension was centrifuged again at 31,100 $\times g$ for 20 min at 4 $^{\circ}$ C. The final pellet was resuspended in ice-cold Tris buffer and stored at -80 $^{\circ}$ C. The protein concentration was determined by the method of Bradford.

S2R Ligand Binding Assay

In vitro S1R ligand binding assays were performed with [³H](+)-pentazocine (26.9 Ci/mmol). Guinea pig brain cortex homogenates (250 µg/sample) were incubated with increasing concentrations of test compounds, [³H](+)-pentazocine (2 nM) and Tris buffer (50 mM, pH 7.4) in a final volume of 0.5 mL, at 37 °C. Unlabeled (+)-pentazocine (10 µM) was used to measure non-specific binding. The K_d value of [³H](+)-pentazocine is 2.9 nM. Bound and free radioligand were separated by fast filtration under reduced pressure using a Millipore filter apparatus through Whatman GF 6 glass fiber filters, which were presoaked in a 0.5% poly(ethyleneimine) water solution for 120 min. Each filter paper was rinsed three times with 3 mL of ice-cold Tris buffer (50 mM, pH 7.4), dried at room temperature, and incubated overnight with 3 mL of Ultima Gold MV Scintillation cocktail into pony vials.

S2R Ligand Binding Assay

In vitro S2R ligand binding assays were carried out with [³H]1,3-di-*o*-tolylguanidine ([³H]DTG, 35.5 Ci/mmol). The thawed membrane preparation of rat liver (250 µg/sample) was incubated with increasing concentrations of test compounds, [³H]DTG (2 nM) in the presence of (+)-pentazocine (5 µM) as S1R masking agent, and Tris buffer (50 mM, pH 8.0) in a final volume of 0.5 mL, at room temperature. Non-specific binding was evaluated with unlabeled DTG (10 µM). The K_d value of [³H]DTG is 17.9 nM. Bound and free radioligand were separated by fast filtration under reduced pressure using a Millipore filter apparatus through Whatman GF 6 glass fiber filters, which were presoaked in a 0.5% poly(ethyleneimine) water solution for 120 min. Each filter paper was rinsed three times with 3 mL of ice-cold Tris buffer (10 mM, pH 8), dried at room temperature, and incubated overnight with 3 mL of scintillation fluid into pony vials.

Data Analysis

The K_i-values were calculated with the program GraphPad Prism[®] 6.0 (GraphPad Software, San Diego, CA, USA). The K_i-values are given as the mean value ± SD from at least two independent experiments performed in duplicate.

3.4.2. Cytotoxicity Studies

Cell Culture

The human neuroblastoma SH-SY5Y (ATCC CRL-2266) cells were maintained in Dulbecco's modified Eagle's medium (DMEM; Gibco, Life Technologies Inc., Frederick, MD, USA) supplemented with 10% (*v/v*) fetal bovine serum (FBS) and antibiotic antimycotic solution (100 U penicillin, 100 µg/mL streptomycin and 0.25 µg/mL amphotericin B; Sigma-Aldrich, St. Louis, MO, USA) at 37 °C in a humidified incubator with a 5% CO₂/95% air atmosphere.

Cell Viability Test

Cell viability was tested by using Resazurin (SERVA Electrophoresis GmbH, Heidelberg, Germany), which in metabolically active cells is reduced to Resufurin, a redox indicator, whose fluorescence is proportional to the number of live cells [43,44]. The stock solution of resazurin sodium salt (440 µM, 10×) diluted in phosphate buffered saline (PBS) was prepared and stored at −20 °C. Working solution (44 µM resazurin) was prepared on the same day of each assay by diluting resazurin stock solution 1:10 in a standard culture medium. After the removal of residual media, 100 µL of a working solution containing 44 µM resazurin diluted in culture medium was added to each well of a p96 black plate.

Cells (5 × 10³), seeded in a black 96-well (clear bottom) plate, were incubated at 37 °C with 44 µM Resazurin solution equal to 10% of the complete medium volume (100 µL DMEM with 10% FCS + 11 µL Resazurin 440 µM).

The fluorescent signal of the resorufin was monitored with excitation λ = 530 nm and emission λ = 590 nm by using an Envision 2104 multi-label microplate reader (Perkin Elmer, Boston, MA, USA). Measurements were performed at time 0 and after 1 h of incubation.

The percentage of viability was calculated after subtraction of the background (obtained by killing the cells), on the basis of the ratio between the fluorescence values of the cells incubated with a compound and the fluorescence values of cells incubated with the solvent (1% DMSO). The viability of cells incubated with 1% DMSO was considered to be equivalent to 100%.

Data Analysis

The statistical analysis was carried out with GraphPad Prism[®] 6.0 (GraphPad Software, Inc, La Jolla, CA, USA) software using an unpaired *t*-test. *p* < 0.05 was considered statistically significant. Cytotoxicity concentrations (IC_{50s}) were determined from dose-response curves analyzed by using GraphPad Prism software.

Real-Time PCR to Test Neuroprotective Properties

Gene expression levels of genes known to be implicated in anti-oxidant response (SOD1 and NRF2) were determined by quantitative Real-Time PCR. SH-SY5Y cells (100.000/well) were seeded in 35 mm plates and incubated for 12 h with the **5e**, **5i**, **5d**, **5o**, **5h**, and **5k**, pentazocine, haloperidol, (12.5 µM) or DMSO (1%) for 12 h. Total RNA was extracted by using Trifast reagent (Euroclone, Milan, Italy), according to the manufacturer's instructions.

Total RNA (500 ng) was primed with hexameric random primers and retrotranscribed into cDNA with M-MLV reverse transcriptase (Thermo Fisher Scientific, Waltham, MA, USA). The normalization of targets' gene expression was performed against the housekeeping gene RPL13A. Real-Time PCRs were performed by using iQ SYBR Green Supermix and CFX96 Real-Time PCR detection system (Bio-Rad Laboratories, Redmond, WA, USA). The relative expression levels were calculated using the $2^{-\Delta\Delta CT}$ method. An unpaired T-test was used to determine statistical significance. Values are presented as mean and error bars indicate standard errors (SE). The results are representative of two independent experiments in triplicate.

Primer pair sequences were the following (5 to 3'): RPL13A_Ex7_Fw, CCTGGAG-GAGAAGAGGAAAGAGA and RPL13A_Ex8_Rv, TTGAGGACCTCTGTGTAATTTGTCAA; hSOD1_ex1_as, TTGCGTCGTAGTCTCCTG, and hSOD1_ex2_as, CACCTTCACTGGTC-CATTAC; NFE2L2_Ex1for, ATCATGATGGACTTGGAGCTG; NFE2L2_Ex2rev, GCTCAT-ACTCTTCCGTCGC.

4. Conclusions

In order to find novel SR modulators with potential neuroprotective effects, we designed, synthesized, and in vitro tested novel ifenprodil analogs, a prototypical GluN2B receptor inhibitor. The synthesized compounds showed a preferential affinity for the S1R subtype, and 6 out of 15 derivatives have Ki S1R values <20 nM, with the piperazine derivative **5h** achieving the highest results (Ki S1R = 1.4 nM, selectivity over S2R = 60).

According to a preliminary in vitro antioxidant assay, four of the best S1R ligands have a greater intrinsic ability to scavenge ABTS-derived radicals and H₂O₂ than Trolox, the reference standard, and have a negligible impact on neuroblastoma SH-SY5Y cell viability.

Our results revealed that two derivatives of the series (**5d** and **5i**) induce an increase in the mRNA levels of the antioxidant NRF2 and SOD1 genes in SH-SY5Y cells, suggesting that they may be useful agents for preventing neurons from suffering from oxidative damage.

Although the precise mechanisms by which S1R can regulate SOD1 and NRF2 expression are not clear, considering that it plays a role in various cellular processes, such as calcium signaling, cell survival, and stress response [45,46], we hypothesize that its stimulation by agonists might regulate gene expression (with neuroprotective effects) through its known translocation to the endoplasmic reticulum, IP3 receptor stabilization, ER stress reduction, and modulation of calcium signaling, such as shown in several other cases [26,47–49].

Supplementary Materials: The following supporting information can be downloaded at: <https://www.mdpi.com/article/10.3390/molecules28083431/s1>, Figure S1: Competition curves for compounds 5e, 5i, 5d, 5o, 5h and 5k in comparison with Haloperidol, NE100 and Siramesine.

Author Contributions: Conceptualization, D.Z. and M.G.M.; methodology, D.Z., M.R., M.D., E.A., A.M., A.C., S.C. and E.A.; software, M.R., M.D., E.A., A.M. and S.F.; validation, D.Z., M.R., S.F., E.A., M.D., A.M. and S.C.; formal analysis, D.Z., A.C., M.R., M.D. and E.A.; investigation, D.Z. and M.R.; resources, D.Z., M.G.M., M.R., E.A., A.M. and S.F.; data curation, D.Z., M.R., A.C., E.A., M.D. and S.F.; writing—original draft preparation, D.Z.; writing—review and editing, D.Z., M.R., S.F. and S.C.; visualization, D.Z.; supervision, D.Z., M.R. and S.C.; project administration, D.Z. and M.G.M.; funding acquisition, D.Z., S.F. and M.G.M. All authors have read and agreed to the published version of the manuscript.

Funding: This research received no external funding.

Institutional Review Board Statement: The experiments were carried out following the ethical provisions established by the directive for animal experiments and were approved by the Ministry of Health (Italy), (authorization no. 385/2021-PR) according to Italian law.

Informed Consent Statement: Not applicable.

Data Availability Statement: The data presented in this study are available on request from the corresponding author.

Acknowledgments: We acknowledge the CINECA Awards N. HP10CKYM0P, 2019 for the availability of high-performance computing resources and support. The financial support of the FRA2021 Research Fund (University of Trieste, owner Daniele Zampieri) is gratefully acknowledged.

Conflicts of Interest: The authors declare no conflict of interest.

Sample Availability: Samples of all synthesized compounds are available from the authors.

References

1. Giacalone, M.; Di Sacco, F.; Traupe, I.; Pagnucci, N.; Forfori, F.; Giunta, F. Chapter 2: Blueberry Polyphenols and Neuroprotection. In *Bioactive Nutraceuticals and Dietary Supplements in Neurological and Brain Disease*; Academic Press: Cambridge, MA, USA, 2015; pp. 17–28.
2. Bogar, F.; Fulop, L.; Penke, B. Novel Therapeutic Target for Prevention of Neurodegenerative Diseases: Modulation of Neuroinflammation with Sig-1R Ligands. *Biomolecule* **2022**, *12*, 363. [[CrossRef](#)] [[PubMed](#)]
3. GBD 2016 Neurology Collaborators. Global, regional, and national burden of neurological disorders, 1990–2016: A systematic analysis for the Global Burden of Disease Study 2016. *Lancet Neurol.* **2019**, *18*, 459–480. [[CrossRef](#)] [[PubMed](#)]
4. Jay, T.R.; Bemiller, S.M.; Neilson, L.E.; Cheng-Hathaway, P.J.; Lamb, B.T. *Neuroinflammation and Neurodegenerative Diseases*; Oxford University Press: Oxford, UK, 2016; Volume 1.
5. MacPherson, K.P.; de Sousa Rodrigues, M.E.; Cintron, A.F.; Tansey, M.G. Neuroinflammation in Age-Related Neurodegenerative Diseases. In *The Molecular and Cellular Basis of Neurodegenerative Diseases*; Elsevier: Amsterdam, The Netherlands, 2018; pp. 477–507; ISBN 978-0-12-811304-2.
6. Di Sabato, D.J.; Quan, N.; Godbout, J.P. Neuroinflammation: The devil is in the details. *J. Neurochem.* **2016**, *139*, 136–153. [[CrossRef](#)] [[PubMed](#)]
7. Korovesis, D.; Rubio-Tomás, T.; Tavernarakis, N. Oxidative Stress in Age-Related Neurodegenerative Diseases: An Overview of Recent Tools and Findings. *Antioxidants* **2023**, *12*, 131. [[CrossRef](#)]
8. Uttara, B.; Singh, A.V.; Zamboni, P.; Mahajan, R.T. Oxidative stress and neurodegenerative diseases: A review of upstream and downstream antioxidant therapeutic options. *Curr. Neuropharmacol.* **2009**, *7*, 65–74. [[CrossRef](#)]
9. Khan, T.A.; Hassan, I.; Ahmad, A.; Perveen, A.; Aman, S.; Quddusi, S.; Alhazza, I.; Ashraf, G.M.; Aliev, G. Recent Updates on the Dynamic Association Between Oxidative Stress and Neurodegenerative Disorders. *CNS Neurol. Disord. Drug Targets* **2016**, *15*, 310–320. [[CrossRef](#)]
10. Korinek, M.; Kapras, V.; Vyklicky, V.; Adamusova, E.; Borovska, J.; Vales, K.; Stuchlik, A.; Horak, M.; Chodounska, H.; Vyklicky, L., Jr. Neurosteroid modulation of N-methyl-d-aspartate receptors: Molecular mechanism and behavioral effects. *Steroids* **2011**, *13*, 1409–1418. [[CrossRef](#)]
11. Clemente, A.S.; Nicoll, R.A.; Roche, K.W. Diversity in NMDA receptor composition: Many regulators, many consequences. *Neuroscientists* **2013**, *19*, 62–75. [[CrossRef](#)]
12. Danysz, W.; Parsons, C.G. Glycine and N-Methyl-D-Aspartate Receptors: Physiological Significance and Possible Therapeutic Applications. *Pharmacol. Rev.* **1998**, *50*, 597–664.

13. Reynolds, I.J.; Miller, R.J. Ifenprodil is a novel type of N-methyl-D-aspartate receptor antagonist: Interaction with polyamines. *Mol. Pharmacol.* **1989**, *36*, 758–765.
14. Maurice, T.; Lockhart, B.P. Neuroprotective and anti-amnesic potentials of sigma (s) receptor ligands. *Prog. Neuro-Psychopharmacol. Biol. Psychiatry* **1997**, *21*, 69–102.
15. King, M.; Pan, Y.X.; Mei, J.; Chang, A.; Xu, J.; Pasternak, G.W. Enhanced kappa-opioid receptor-mediated analgesia by antisense targeting the sigma1 receptor. *Eur. J. Pharmacol.* **1997**, *331*, R5–R6. [[CrossRef](#)] [[PubMed](#)]
16. Modell, S.; Nober, D.; Holzbach, R. Efficacy and safety of an opiate sigma receptor antagonist (SL 82.0715) in schizophrenic patients with negative symptoms: An open dose-range study. *Pharmacopsychiatry* **1996**, *29*, 63–66. [[CrossRef](#)]
17. Huber, M.T.; Gotthardt, U.; Schreiber, W.; Krieg, J.C. Efficacy and safety of the sigma receptor ligand EMD 57445 (panamesine) in patients with schizophrenia: An open clinical trial. *Pharmacopsychiatry* **1999**, *32*, 68–72. [[CrossRef](#)] [[PubMed](#)]
18. McCracken, K.A.; Bowen, W.D.; Walker, F.O.; De Costa, B.; Matsumoto, R.R. Two novel sigma receptor ligands, BD1047 and LR172, attenuate cocaine-induced toxicity and locomotor activity. *Eur. J. Pharmacol.* **1999**, *370*, 225–232. [[CrossRef](#)]
19. Kato, K.; Hayako, H.; Ishihara, Y.; Marui, S.; Iwane, M.; Miyamoto, M. TAK-147, an acetylcholinesterase inhibitor, increases choline acetyltransferase activity in cultured rat septal cholinergic neurons. *Neurosci. Lett.* **1999**, *260*, 5–8. [[CrossRef](#)]
20. Vecchio, L.; Sorrentino, A.; Paoletti, R.; Marra, M.; Arbitrio, M. The State of The Art on Acetylcholinesterase Inhibitors in the Treatment of Alzheimer’s Disease. *J. Cent. Nerv. Syst. Dis.* **2021**, *13*, 11795735211029112. [[CrossRef](#)] [[PubMed](#)]
21. Zampieri, D.; Fortuna, S.; Cassina, A.; Amata, E.; Dichiaro, M.; Marrazzo, A.; Calabretti, A.; Mamolo, M.G. New Ifenprodil analogues as neuroprotective agents. In Proceedings of the XXVII National Meeting in Medicinal Chemistry, Bari, Italy, 11–14 September 2022.
22. Zampieri, D.; Fortuna, S.; Calabretti, A.; Romano, M.; Menegazzi, R.; Schepmann, D.; Wunsch, B.; Collina, S.; Zanon, D.; Mamolo, M.G. Discovery of new potent dual sigma receptor/GluN2b ligands with antioxidant property as neuroprotective agents. *Eur. J. Med. Chem.* **2019**, *180*, 268–282. [[CrossRef](#)]
23. Daina, A.; Michielin, O.; Zoete, V. SwissADME: A free web tool to evaluate pharmacokinetics, drug-likeness and medicinal chemistry friendliness of small molecules. *Sci. Rep.* **2017**, *7*, 42717. [[CrossRef](#)]
24. Lipinski, C.A. Lead and drug-like compounds: The rule-of-five revolution. *Drug Discov. Today Technol.* **2004**, *1*, 337–341. [[CrossRef](#)]
25. King, L.C.; Ostrum, G.K. Selective bromination with copper (II) bromide. *J. Org. Chem.* **1964**, *29*, 3459–3461. [[CrossRef](#)]
26. Sałaciak, K.; Pytka, K. Revisiting the sigma-1 receptor as a biological target to treat affective and cognitive disorders. *Neurosci. Biobehav. Rev.* **2022**, *132*, 1114–1136. [[CrossRef](#)] [[PubMed](#)]
27. Naia, L.; Pinho, C.M.; Dentoni, G.; Liu, J.; Leal, N.S.; Ferreira, D.M.S.; Schreiner, B.; Filadi, R.; Fão, L.; Connolly, N.M.C.; et al. Neuronal cell-based high-throughput screen for enhancers of mitochondrial function reveals luteolin as a modulator of mitochondria-endoplasmic reticulum coupling. *BMC Biol.* **2021**, *24*, 57. [[CrossRef](#)] [[PubMed](#)]
28. Wang, J.; Zhao, J.; Cui, X.; Mysona, B.A.; Navneet, S.; Saul, A.; Ahuja, M.; Lambert, N.; Gazaryan, I.G.; Thomas, B.; et al. The molecular chaperone sigma 1 receptor mediates rescue of retinal cone photoreceptor cells via modulation of NRF2. *Free Radic. Biol. Med.* **2019**, *134*, 604–616. [[CrossRef](#)] [[PubMed](#)]
29. Wang, J.; Xiao, H.; Barwick, S.R.; Smith, S.B. Comparison of sigma 1 receptor ligands SA4503 and PRE084 to (+)-Pentazocine in the rd10 mouse model of RP. *Investig. Ophthalmol. Vis. Sci.* **2020**, *61*, 3. [[CrossRef](#)]
30. Lasbleiz, C.; Peyrel, A.; Tarot, P.; Sarniguet, J.; Crouzier, L.; Cubedo, N.; Delprat, B.; Rossel, M.; Maurice, T.; Liévens, J.C. Sigma-1 receptor agonist PRE-084 confers protection against TAR DNA-binding protein-43 toxicity through NRF2 signalling. *Redox Biol.* **2022**, *58*, 102542. [[CrossRef](#)]
31. Pal, A.; Fontanilla, D.; Gopalakrishnan, A.; Chae, Y.K.; Markley, J.L.; Ruoho, A.E. The sigma-1 receptor protects against cellular oxidative stress and activates antioxidant response elements. *Eur. J. Pharmacol.* **2012**, *682*, 12–20. [[CrossRef](#)]
32. Schmidt, H.R.; Zheng, S.; Gurpinar, E.; Koehl, A.; Manglik, A.; Kruse, A.C. Crystal structure of the human $\sigma 1$ receptor. *Nature* **2016**, *532*, 527. [[CrossRef](#)]
33. Stewart, J.J.P. Mopac-A semiempirical molecular-orbital program. *J. Comput. Aided Mol. Des.* **1990**, *4*, 1–45. [[CrossRef](#)]
34. Trott, O.; Olson, A.J. AutoDock Vina: Improving the speed and accuracy of docking with a new scoring function, efficient optimization, and multithreading. *J. Comput. Chem.* **2010**, *31*, 455–461. [[CrossRef](#)]
35. Wang, J.; Wolf, R.M.; Caldwell, J.W.; Kollman, P.A.; Case, D.A. Development and testing of a general amber force field. *J. Comput. Chem.* **2004**, *25*, 1157–1174. [[CrossRef](#)] [[PubMed](#)]
36. Batista, P.R.; Wilter, A.; Durham, E.H.A.B.; Pascutti, P.G. Molecular dynamics simulations applied to the study of subtypes of HIV-1 protease common to Brazil, Africa, and Asia. *Cell Biochem. Biophys.* **2006**, *44*, 395–404. [[CrossRef](#)] [[PubMed](#)]
37. Hess, B.; Bekker, H.; Berendsen, H.J.C.; Fraaije, J.G.E.M. LINCS: A linear constraint solver for molecular simulations. *J. Comput. Chem.* **1997**, *18*, 1463–1472. [[CrossRef](#)]
38. Daura, X.; Gademann, K.; Jaun, B.; Seebach, D.; van Gestreen, W.F. Peptide folding: When simulation meets experiment. *Angew. Chemie Int. Ed.* **1999**, *38*, 236–240. [[CrossRef](#)]
39. Pronk, S.; Pall, S.; Schulz, R.; Larsson, P.; Bjekmar, P.; Apostolov, R.; Shirts, M.R.; Smith, J.C.; Kason, P.M.; Van der Spoel, D.; et al. GROMACS 4.5: A high-throughput and highly parallel open-source molecular simulation toolkit. *Bioinformatics* **2013**, *29*, 845–854.
40. Valdés-Tresanco, M.S.; Valdés-Tresanco, M.E.; Valiente, P.A.; Moreno, E. gmx_MMPBSA: A new tool to perform end-state free energy calculations with GROMACS. *J. Chem. Theory Comput.* **2021**, *17*, 6281–6291. [[PubMed](#)]

41. Re, R.; Pellegrini, N.; Proteggente, A.; Pannala, A.; Gang, M.; Rice-Evans, C. Antioxidant activity applying an improved ABTS radical cation decolorization assay. *Free Rad. Biol. Med.* **1999**, *26*, 1231–1237. [[CrossRef](#)] [[PubMed](#)]
42. Bradford, M.M. A Rapid and sensitive Method for the Quantitation of Microgram Quantities of Protein Utilizing the Principle of Protein-Dye Binding. *Anal. Biochem.* **1976**, *72*, 248–254.
43. O'Brien, J.; Wilson, I.; Orton, T.; Pognan, F. Investigation of the Alamar Blue (resazurin) fluorescent dye for the assessment of mammalian cell cytotoxicity. *Eur. J. Biochem.* **2000**, *267*, 5421–5426.
44. Uzarski, J.S.; DiVito, M.D.; Wertheim, J.A.; Miller, W.M. Essential design considerations for the resazurin reduction assay to noninvasively quantify cell expansion within perfused extracellular matrix scaffolds. *Biomaterials* **2017**, *129*, 163–175. [[CrossRef](#)]
45. Lachance, V.; Bélanger, S.M.; Hay, C.; Le Corvec, V.; Banouvang, V.; Lapalme, M.; Tarmoun, K.; Beaucaire, G.; Lussier, M.P.; Kourrich, S. Overview of Sigma-1R Subcellular Specific Biological Functions and Role in Neuroprotection. *Int. J. Mol. Sci.* **2023**, *24*, 1971. [[CrossRef](#)] [[PubMed](#)]
46. Hayashi, T. The Sigma-1 Receptor in Cellular Stress Signaling. *Front. Neurosci.* **2019**, *13*, 733. [[CrossRef](#)] [[PubMed](#)]
47. Decuypere, J.P.; Monaco, G.; Missiaen, L.; De Smedt, H.; Parys, J.B.; Bultynck, G. IP(3) Receptors, Mitochondria, and Ca Signaling: Implications for Aging. *J. Aging Res.* **2011**, *2011*, 920178. [[CrossRef](#)] [[PubMed](#)]
48. Bahar, E.; Kim, H.; Yoon, H. ER Stress-Mediated Signaling: Action Potential and Ca(2+) as Key Players. *Int. J. Mol. Sci.* **2016**, *17*, 1558. [[CrossRef](#)] [[PubMed](#)]
49. Berridge, M.J.; Bootman, M.D.; Roderick, H.L. Calcium signalling: Dynamics, homeostasis and remodelling. *Nat. Rev. Mol. Cell Biol.* **2003**, *4*, 517–529. [[CrossRef](#)] [[PubMed](#)]

Disclaimer/Publisher's Note: The statements, opinions and data contained in all publications are solely those of the individual author(s) and contributor(s) and not of MDPI and/or the editor(s). MDPI and/or the editor(s) disclaim responsibility for any injury to people or property resulting from any ideas, methods, instructions or products referred to in the content.